ICAS 2016
30th Congress of the International Council of the Aeronautical Sciences
DCC, Daejeon, Korea ; September 25-30, 2016

AN EXPERIMENTAL INVESTIGATION ON THE FREESTREAM TURBULENCE UPSTREAM OF A SWEPT WING

Isabella Fumarola*
***City University London**

Keywords: *freestream turbulence, swept wing, leading edge, vorticity*

Abstract

A considerable amount of theoretical and experimental research exists on the amplification of vorticity at the edge of the boundary layer near the stagnation point in two-dimensional flows. Experiments on cylinders, flat plates and wings have confirmed the theory of vorticity amplification. Here, the phenomenon is investigated when a sweep angle is added to the model, introducing a spanwise velocity component parallel to the leading edge. Two experimental investigations are presented, one on a straight cylinder and one on a swept wing NACA0050. The aim is to measure variations of the fluctuating component of the velocity close to the leading edge, investigating the difference between a swept and an unswept case. The experiments were carried out using two-dimensional Laser Doppler Anemometers (LDA), which measure two components of the velocity. For the cylinder, the behaviour of the fluctuating components confirms the predictions of the theory. In the case of the swept swing, where no systematic theory is available, a distinctive but less organized amplification of vorticity has been observed.

1 Introduction and motivation

In 1928 Piercy and Richardson [1] found that the region upstream of the leading edge of an aerofoil is a centre of disturbances in which a high level of turbulence intensity is established. This observation has been theoretically demonstrated by Sutera et al. through their "vorticity amplification theory" in 1963 [2, 3] and subsequently experimentally validated by many authors. The theory superimposes a sinusoidal perturbation onto the incoming flow and analyses how the stretching and tilting of the vortex tubes is thus created. The vorticity is amplified only if properly oriented and if the wavelength is greater than the *natural wavelength* λ_0, which depends on the geometry of the body and on the flow condition.

A first experimental investigation was carried out by Sadeh et al. [4] on a stagnation flat plate. The mean velocity and the fluctuating component, in the freestream direction, were measured using a hot-wire anemometer. In agreement with the theory, the experiment revealed an increase in the fluctuating component of the velocity at the edge of the boundary layer. In the same experiment, a flow visualization using smoke exhibited the presence of coherent structures at the edge of the boundary layer. To prove that those structures are related to the oncoming freestream turbulence, Sadeh et al. repeated the experiment by inserting different grids in the wind tunnel ahead of the model. The amplification was in some cases even higher than 100%.

Lately, many experiments have reported the same phenomenon on several bodies. Sadeh et al. [5] found amplification up to ~255% on a cylinder; Bearman studied a wing with a blunt leading edge [6]; Sadeh and Sullivan observed the structures on a NACA65-010 aerofoil [7].

Independently, mathematicians Kerr and Dold carried out a comprehensive theoretical investigation of the same problem in 1994 [8]. They analysed the stagnation point flow in the situation where a steady periodic perturbation is superimposed to the Hiemenz-flow solution. For the latter case, they found an exact solution to the Navier Stokes equation that shows an array of rotating-vortices at the edge of the stagnation point boundary layer.

From this brief review of the literature, it is shown that the vorticity amplification has been widely studied in the case of two-dimensional flows. The problem studied in this work is the behaviour of the vortices when a sweep angle is added to the model, that is, what happens to those vortices when the flow has also a spanwise component at the leading edge. In order to study the phenomenon two component Laser Doppler Anemometer (LDA) measurements have been carried out on a swept model.

The attachment line of a swept wing plays a crucial role in establishing the initial conditions for the downstream flow. One phenomenon it affects is the transition from laminar to turbulent boundary layer [9]. The process of boundary layer receptivity is influenced by several external parameters. In particular, it is known that the freestream turbulence influences the transition on swept wings [10], but the physical mechanism of interaction between freestream turbulence and boundary layer is still unknown. It cannot yet be stated whether the vortices created at the attachment line have a role in the receptivity process, but the study of the interaction between freestream turbulence and leading edge flow may be of help in understanding this and other phenomena.

In this paper, two different experiments are presented. The first one is on a straight cylinder, a case already known in the literature. Its aim is to provide a comparison between a swept and an unswept case and to validate the methodology employed here. The second experiment is on a swept wing, NACA0050. Both experiments have been carried out in the same wind tunnel, using two components Laser Doppler Anemometry to measure the mean and the fluctuating velocity component.

2 Background

2.1 Swept Hiemenz flow

An exact solution of the flow impinging on a surface was presented by Hiemenz in 1911 [11]. Assume a two-dimensional infinity plate is placed in the YZ-plane, and define the X-coordinate as perpendicular to this plane, starting from the stagnation point going towards the freestream. The flow is coming along X, and is defined by $\overrightarrow{Q_\infty} = (U_\infty, 0, 0)$. The velocity decreases approaching the wall and the flow is split in two alternatives direction $\pm$Y at the wall.

This is represented by an inviscid solution of the Navier Stokes equations:

$$\begin{cases} u = aX, \\ w = -aY, \\ v = 0, \end{cases}$$

where a is a constant that depends on the external flow and on the geometry of the body.

Now, suppose the model is placed with a sweep angle Λ (figure1), and define a local coordinate system (x,y,z) such that x is perpendicular to the leading edge, z is along the attachment line and y is perpendicular, as shown in figure 1. The external flow field expressed in the local coordinate system becomes $\mathrm{Q}_\infty = (\mathrm{U}_\infty, 0, \mathrm{V}_\infty)$, where $\mathrm{U}_\infty = \mathrm{Q}_\infty \cos(\Lambda)$ and $\mathrm{V}_\infty = Q_\infty \sin(\Lambda)$.

The inviscid solution leads to:

$$\begin{cases} u = ax, \\ w = -ay, \\ v = const, \end{cases}$$

where the u becomes small as the body is approached, the w-component increases far from y=0 and the v-component remains constant along the leading edge.

The viscous solution can be numerically calculated from the Falkner-Scan-Cooke equations [12]:

$$f''' + ff'' - f'^2 + 1 = 0,$$
$$g'' + fg' = 0,$$

where f and g are defined by:

$$\begin{cases} u(\eta) = f'(\eta), \\ w(\eta) = 0, \\ v(\eta) = g(\eta), \end{cases}$$

and η is the dimensionless coordinate $\eta = \sqrt{\frac{U(\beta+1)}{2\nu x}}$ in which β is a constant equal to unity for the Hiemenz flow.

The Hiemenz flow has proven to be a good approximation of the flow at the attachment line [12].

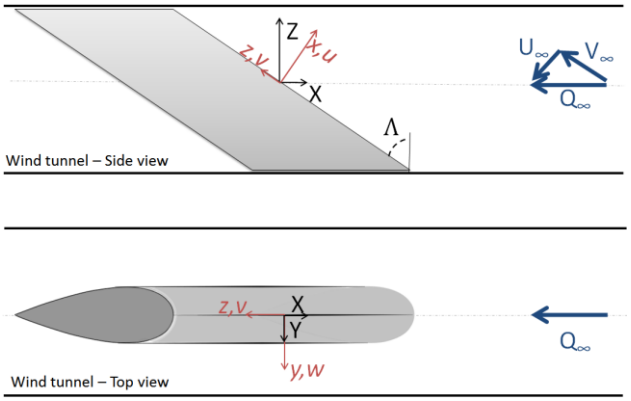

Figure 1 Swept wing in the wind tunnel. (X,Y,Z) is the coordinate system of the wind tunnel, (*x*,*y*,*z*) the coordinate system aligned with the flow and (*u*,*v*,*w*) the flow velocity components. Q_∞ is the external flow, U_∞ and V_∞ its projections on the flow coordinate system.

2.2 Vorticity amplification theory

The vorticity amplification theory considers a case very similar to the Hiemenz flow. The oncoming flow is described with a superimposed disturbance that, in the first approximation, follows a sinusoidal pattern defined by a wavelength λ.

The problem was studied independently by Sutera et. al [2] [3] and Kerr et al. [8]. The method used in the two cases is slightly different, but the solution found is the same. In the first case, a periodic behaviour along y is superimposed to the flow approaching a two-dimensional body. This is then substituted inside the transport equation and the time-independent energy transport equation. The Hiemenz flow is substituted as a boundary condition. This leads to equations that are solved numerically.

In the second case, Kerr and Dold start from the Hiemenz flow solution and superimpose a perturbation along the y-direction. Substituting in the Navier Stokes equations, they found a non-linear equation. The problem is solved by seeking periodic solutions, and the analysis is concluded by extracting the asymptotic behaviour of the solutions.

Both methods prove that, if the vorticity in the oncoming flow is appropriately oriented and if the wavelength is greater than a certain natural wavelength (λ_0), no matter how small the initial intensity is, the vortex tubes are stretched and this leads to a magnification of the vorticity at the edge of the boundary layer. The vorticity on wavelengths greater than this scale increases in amplitude, due to the stretching, more rapidly than it is dissipated by viscous action.

The natural vorticity wavelength is given by $\lambda_0 = 2\,\pi \left(\frac{\nu}{a}\right)^{1/2}$, where a is again the Hiemenz flow parameter and ν is the kinematic viscosity.

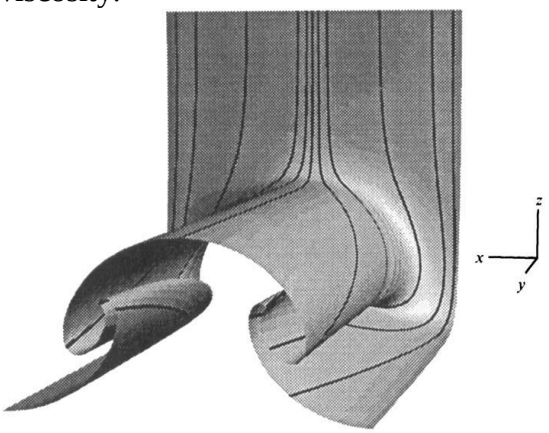

Figure 2 Counter-rotating vortices at the stagnation point on an unswept flat plate, after Kerr **[8]**.

Although in the theory the oncoming perturbation is assumed steady, the resulting vortices evolve in time [5]. Therefore, experimentally they can be observed in the fluctuating component of the velocity.

3 Experiments

3.1 Experimental setup

The experiment has been carried out in the T2 wind tunnel at the Handley Page Laboratory

at City University London which has a speed range between from 4 to 55 m/s.

For this experiment, only one screen was placed ahead of the contraction and the freestream turbulence is 0.8%.

The experimental setup is shown in figure 3. Velocity and temperature in the wind tunnel have been measured using a pitot tube and a thermocouple through a National Instrument system and LabVIEW software. For both experiments the measurements have been performed using two-component Laser Doppler Anemometers with a single head in a coincident mode.

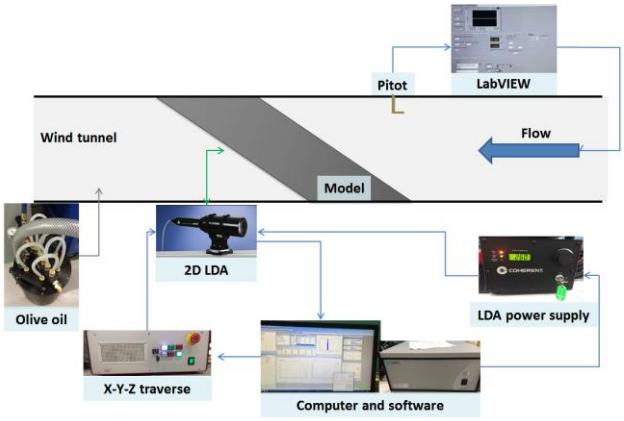

Figure 3 Overview of the experimental setup.

The four laser beams can to measure two velocity components on the same plane. The properties of the two couples of laser beams are shown in table 1.

Laser beams	Wavelength	Probe volume
Green	514.2 mm	dx=0.122 mm dy=2.641 mm dz=0.122 mm
Blue	488 mm	dx=0.122 mm dy=2.641 mm dz=0.122 mm

Table 1 LDA parameters.

The laser comes in from the side of the wind tunnel and can be moved using a traverse system. The laser support allows to rotate the probe around all three axes and this allows to orient the angles of the laser beams to improve the quality of measurements. For both experiments, the laser beams have been oriented parallel to the leading edge of the model.

The lasers' power supply has an input power that can be adjusted up to 600mW, but for the present experiments it was set to 270 mW. Both couples of laser beams include one that is shifted by 40MHz; this enabling the direction of the velocity to be found using a Bragg cell.

The seeding particles used for the experiments are atomized olive oil.

In both experiments the maximum sampling time has been set to 5s with a maximum number of samples at 50000. For the whole duration of the experiment, the data rate was kept in a range that goes from approximately 1 kHz close to the wall inside the boundary layer up to 10 kHz in the freestream.

3.2 Experiment on a cylinder

The model used is a Perspex cylinder with a radius of 75 mm mounted vertically inside the wind tunnel and covering the whole height of the test section, as shown in figure 4. The experiment has been carried out at 7.2 m/s, which corresponds to a Reynolds number $\mathrm{Re_D} = \frac{\mathrm{U_\infty D}}{\nu} \sim 7.14 \cdot 10^4$ based on the diameter of the cylinder.

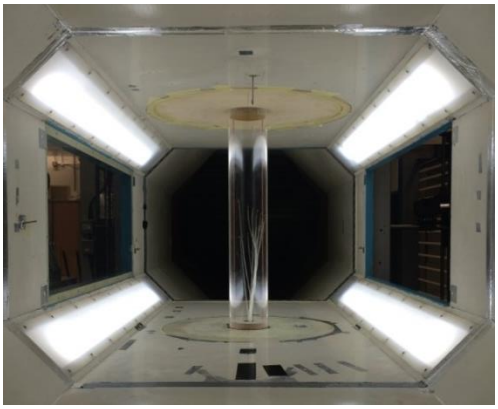

Figure 4 Experiment on the cylinder.

The boundary layer thickness for the Hiemenz flow is $\delta = \sqrt{\nu/a} \sim 0.72$ mm, and the natural wavelength according to the vorticity amplification theory is $\lambda_0 \sim 1.76$ mm.

The velocity components measured in the experiment are U in the streamwise direction

and V in the direction parallel to the cylinder axis. In the coordinate system used for our wind tunnel they correspond to the X and Z directions (see figure 1).

The lasers have been aligned with the leading edge of the cylinder at a distance of 300 mm from the wind tunnel's floor. The Y-axis has been aligned with the flow so that Y=0 corresponds to the stagnation point and X=0 is the closest point to the cylinder that the laser can reach before the signal becomes too noisy. The offset from the wall (X=0) has been corrected in the post-processing with a linear interpolation of the boundary-layer profile.

In figure 5, a comparison with the theoretical potential flow coming through the leading edge of a cylinder is presented.

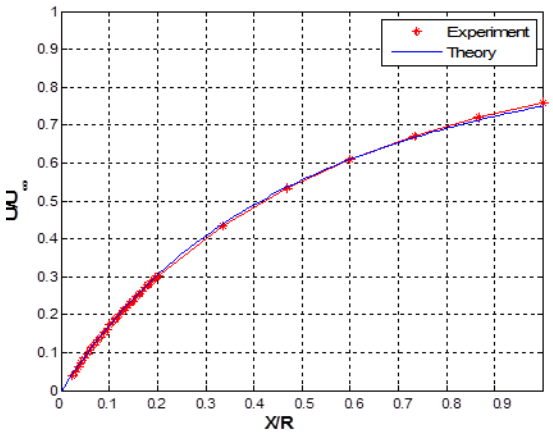

Figure 5 Experiment on the cylinder: U-component of the velocity normalized with the freestream U_∞ versus X normalized with the radius of curvature R.

Two different types of LDA scans have been carried out: one on an X-Y plane and one on an X-Z plane.

In figure 6 and 7, the velocity and the Root Mean Square (RMS) of the velocity are reported in the X-Y plane at Z=0 mm. The measurement points go from Y=-1.5 to +1.5 mm and from X=0 to 5 mm with a constant spatial resolution of 0.2 mm in both directions. As expected, the V component is almost zero everywhere whilst the U component steadily tends to zero on the model. Since measurement area is small, the effect of the curvature is not evident in the U component.

The fluctuating components of the velocity display an increase of intensity with a maximum around the edge of the boundary layer (the dashed line in figure 6 and 7). In figure 7 the RMS is normalized with respect to the freestream total RMS, measured at 200 mm from the leading edge.

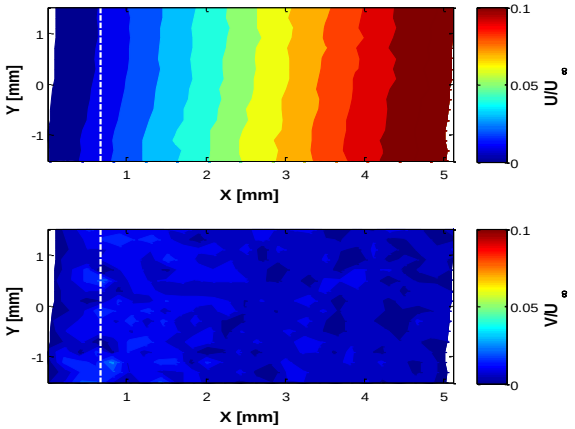

Figure 6 Experiment on the cylinder: velocity on an X-Y plane. The dashed line represents the theoretical boundary layer thickness.

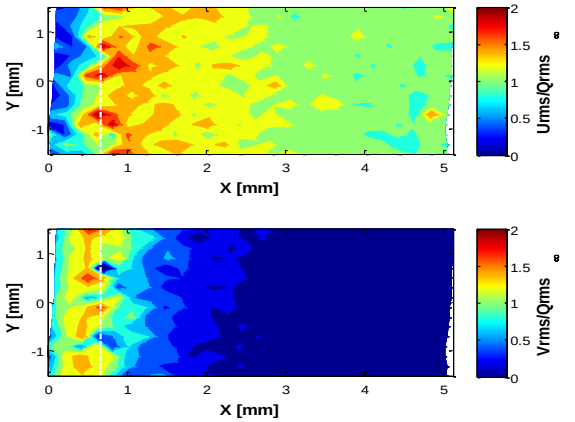

Figure 7 Experiment on the cylinder: normalized U and V RMS on an X-Y plane. The dashed line represents the theoretical boundary layer thickness.

As shown in figure 8, the magnitudes of the two velocity components have been added together. The result shows that the maximum intensity is aligned with the boundary layer edge and it is two times the freestream RMS.

In figure 9 and 10, the same analysis is performed in the X-Z plane at Y=0 mm. The measured area goes from Z=0 to +3 mm and from X=0 to 5 mm with a constant spatial resolution of 0.2 mm for both axes.

Just as has been observed in the case of the X-Y plane, here too the U velocity decreases, and the V component is almost zero

everywhere. The RMS of the velocity increases going towards the model, with a maximum that is at a different location for U and V components.

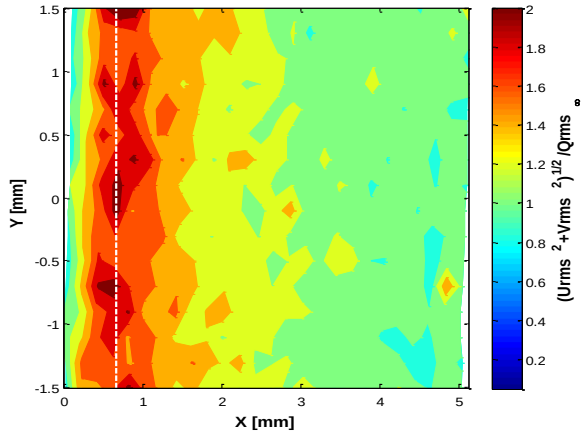

Figure 8 Experiment on the cylinder: total RMS normalized on an X-Y plane.

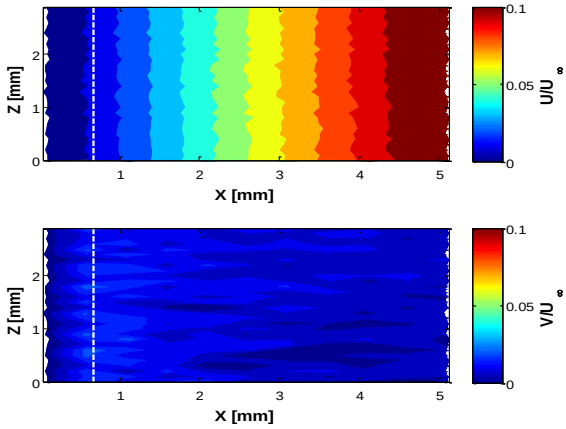

Figure 9 Experiment on the cylinder: velocity on an X-Z plane.

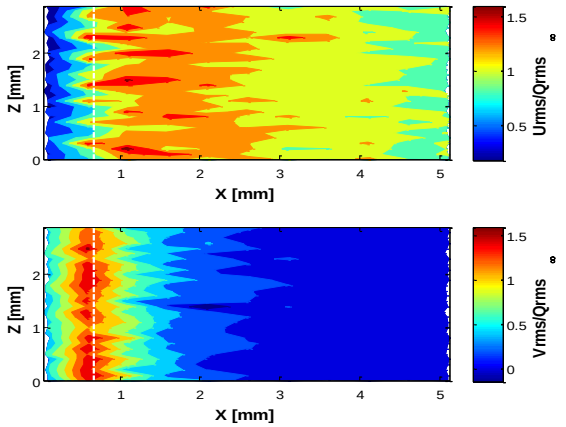

Figure 10 Experiment on the cylinder: normalized RMS of the velocity on an X-Z plane.

Once the two RMS velocity components are added together and normalized with respect to the freestream (figure 11), the maximum (twice the freestream RMS) is again at the edge of the boundary layer.

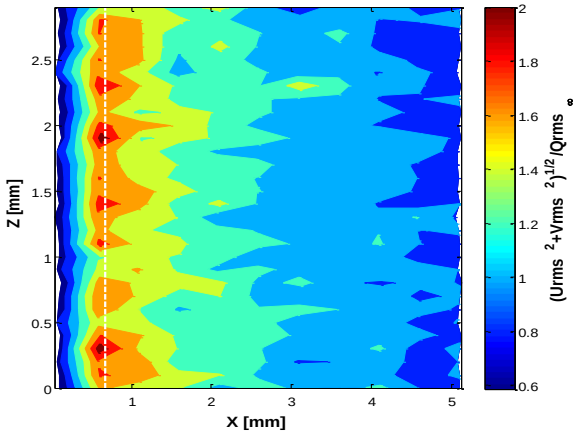

Figure 11 Experiment on the swept wing: total RMS of the velocity on an X-Z plane at Y=0mm.

It is also interesting to notice the spatial distribution of the RMS velocity along the Z-axis at the edge of the boundary layer, with alternate areas of maximum and minimum intensity. This is in agreement with the counter-rotating vortices (figure 2) predicted by the vorticity amplification theory.

3.3 Experiment on a swept wing

The model is a wooden black-painted NACA0050 aerofoil, figure 12. The leading-edge radius is 114 mm, with a chord-length of 466 mm, and a sweep angle of 60°. The model, previously used by Gowree [14], was initially designed to study attachment-line contamination and therefore the dimensions of the model have been optimized to have a thick boundary layer at the leading edge. In order to avoid separation, 9 vortex generators per side have been placed along the symmetrical body of the swept wing.

To check the alignment of the model with respect to the oncoming flow, flow visualizations with fluorescent tufts and measurements of the pressure distribution on the wing have been carried out.

In this experiment, the velocity has been kept constant at 7 m/s for the whole duration of the experiment, so that it corresponds to an

attachment-line Reynolds number $\overline{\mathrm{Re}} = \frac{V_\infty \eta}{\nu} \sim 207$, which is low enough to avoid attachment-line contamination ($\overline{\mathrm{Re}} < 245$) according to Pfenninger [15], Gaster [16], and Poll [17]. The momentum thickness is $\theta = \frac{0.4042\,\nu\,\overline{\mathrm{Re}}}{V_\infty} \sim 0.2095$ mm and the boundary layer thickness $\delta \sim 1.55$ mm.

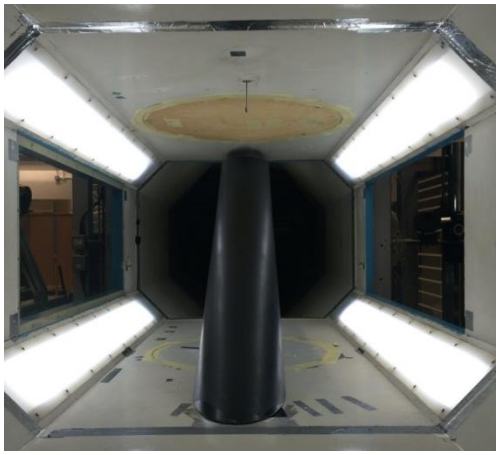

Figure 12 Experiment on the swept wing NACA 0050.

As shown in figure 1, XYZ are the coordinates with respect to the wind tunnel, the streamwise velocity U and the spanwise velocity V have been resolved with respect to the local xyz coordinate system.

The laser beams were aligned approximately at a distance of 700 mm along the leading edge from the bottom of the wind tunnel.

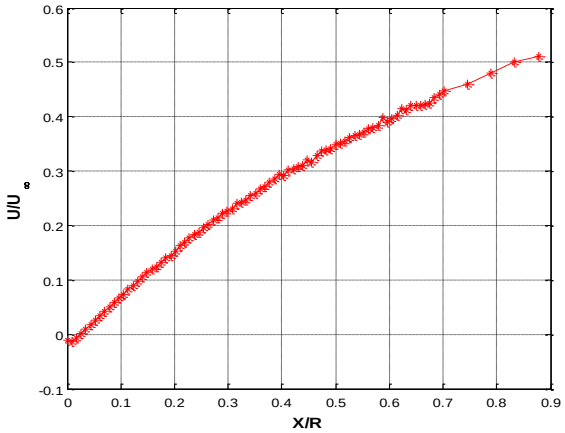

Figure 13 Experiment on the swept wing: U-component of the velocity normalized with the freestream U versus X normalized with the radius of curvature R.

The Y and X axes were aligned in the same way as for the cylinder and the X axis has been shifted in the post-processing using a linear interpolation to find the wall. Figure 13 displays the U velocity from the leading edge up to 100 mm away from the model. The window of the wind tunnel limits the measurement region available, therefore the freestream could not be reached. Already at 100 mm away from the model, the streamlines are curved. It should be considered that the considerable size of the model causes blockage effects in the wind tunnel.

At the leading edge, an effective sweep angle of approximately 62° has been found

Data on the V velocity inside the boundary layer has been compared with the numerical solution of the Falkner-Scan-Cooke equations. Figure 14 shows a good agreement with the predicted flow. In the figure, the V component is normalized by the velocity at the edge of the boundary layer and the x-coordinate is expressed in the dimensionless form $\eta = x\sqrt{\frac{V}{R\nu}}$.

Just as with the cylinder, two types of measurements have been made, lying in the X-Y and in the X-Z plane.

In figures 15 and 16, the X-Z scan at the attachment line Y=0 mm is shown. The measurement points are from 0 to 4 mm along Z and, at X=0 mm, from the leading edge up to 4 mm along X; the resolution in both axes is 0.1 mm.

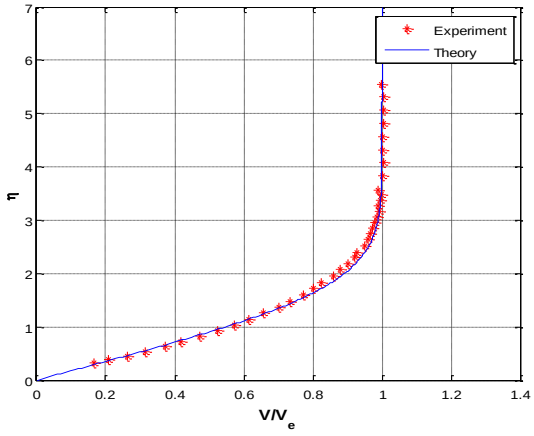

Figure 14 Comparison between measurements of the V component and the Falkner-Skan-Cooke solution.

In figure 15, the V-component decreases going towards the leading edge. So does the U

velocity, although it is of small intensity and this enhances the role of fluctuations. The distribution along Z is uniform everywhere, which is in agreement with the infinite swept condition.

The RMS is reported in figure 16, normalized with respect to the total freestream RMS measured at 200 mm from the leading edge. The amplification in the U component rises up to 1.4 times, while the V component goes up to 1 times starting from lower values respect to the total freestream RMS. Structures along the attachment line are not clearly defined, but a regions of high and low amplification are detected at the edge of the boundary layer.

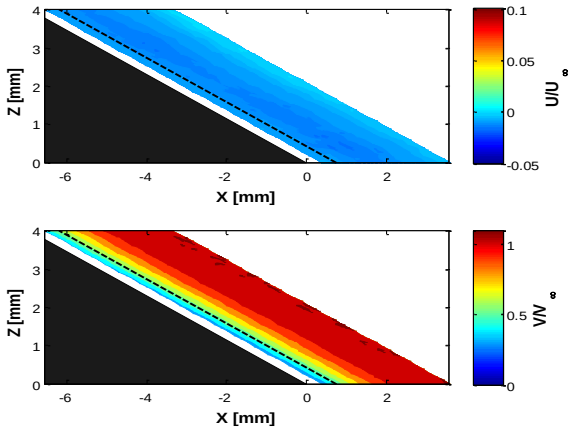

Figure 15 Experiment on the swept wing: U and V velocity, normalized with respect to the freestream, on an X-Z plane. In black is the wing body, while the black dashed line represents the theoretical boundary layer thickness.

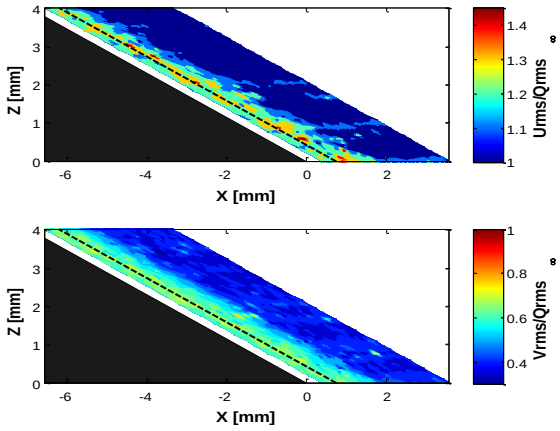

Figure 16 Experiment on the swept wing: RMS of the velocity on an X-Z plane. In black is the wing body, while the black dash line represents the theoretical boundary layer thickness.

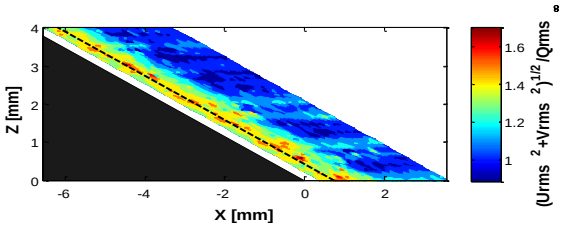

Figure 17 Experiment on the swept wing: total RMS of the velocity in an X-Z plane. The black area represent the body, while the black dashed line stands for the theoretical boundary layer thickness.

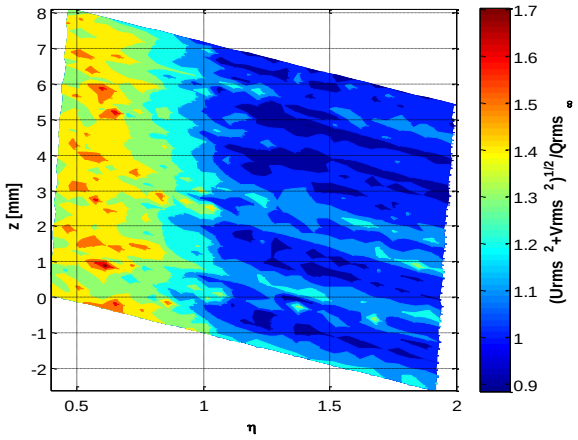

Figure 18 Experiment on the swept wing: RMS of the velocity in the flow coordinate system with x in the dimensionless form.

Figures17 shows the sum of the two magnitude of the RMS velocity vector in the X-Z. While, figure 18 shows the same plot in the flow coordinate system (figure 1) and x is expressed as the dimensionless form η.

The striations far from the boundary layer are not aligned with the flow. As the difference is small, they are likely to be a nonphysical effect due to the measurement.

The area of increase of turbulence in the flow-coordinate system contains patches of high amplified and low amplified regions. This are likely to be physically relevant, as the scenario is similar to the two dimensional case, though less defined.

In figure 19, the velocity in the X-Y scan at Z=0 mm is reported. The X-axis ranges from 0 to 3 mm and the Y-axis from -3 to +3 mm, both with a resolution of 0.2 mm.

As expected, an increase of RMS velocity near the edge of the boundary layer is found also in this plane. It cannot be compared directly to the two-dimensional case, since only a plane

aligned with the flow would be directly comparable.

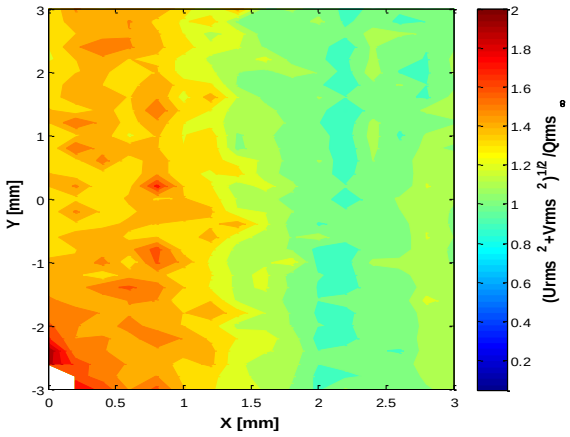

Figure 19 Experiment on the swept wing: RMS of the velocity in an X-Y plane.

4 Conclusions

In this paper, an analysis of the amplification of the freestream turbulence at the edge of the boundary layer has been performed on an unswept cylinder and a swept wing, using Laser Doppler Anemometry.

Measurements on the cylinder are in agreement with previous experiments and theory. In addition, the present experiment has been able to provide a more complete picture of the flow field, with measurements of the two velocity components extending to a wider region both along the axis of the cylinder and along the cross-direction.

An area of increased turbulence at the edge of the boundary layer has been found, with an organization in increased and reduced intensity along the direction parallel to the axis of the cylinder that is in agreement with the theory.

An experiment on a swept wing has also been presented to investigate what happens to the vortices when a velocity component along the attachment line is added to the flow field.

Data on the fluctuating components of the velocity have revealed the existence of higher turbulence region close to the wall. The amplification is similar to the one on the cylinder and goes up to two times the freestream fluctuating component.

Further analysis will be necessary to comprehend better the phenomenon on the swept wings.

The next step would be to compare the spatial distribution of the fluctuating velocity component with the natural wavelength predicted from the two dimensional vorticity amplification theory and to insert different grids upstream of the body to investigate how the amplification is influenced by the spatial distribution of the freestream turbulence.

The influence of the sweep angle of the model on the vorticity amplification should also be studied. A theoretical investigation using the same approach as the two dimensional case is necessary to predict and understand the problem.

Acknowledgements

I would like to acknowledge the support of InnovateUK under grant ref. 113024, Enhanced Fidelity Transonic Wing, led by Airbus. I would also like to thank my PhD supervisors Professor M. Gaster and Professor C. J. Atkin.

References

[1] N.A.V Piercy, E.G. Richardson. The variation of velocity amplitude close to the surface of a cylinder moving through a viscous fluid. *The London, Edinburgh, and Dublin Philosophical Magazine and Journal of Science*, pp. 6(39), 970-977, 1928.

[2] S. P. Sutera, P. F. Maeder, J. Kestin. On the sensitivity of heat transfer in the stagnation-point boundary layer to free-stream vorticity. *Journal of Fluid Mechanics*, vol. 16.04, pp. 497-520, 1963.

[3] S. Sutera. Vorticity amplification in stagnation-point flow and its effect on heat transfer. *Journal of Fluid Mechanics*, vol. 21.03, pp. 513-534, 1965.

[4] S. W. Sadeh, S. P. Sutera, P. F. Maeder. An investigation of vorticity amplification in stagnation flow. *Zeitschrift für Angewandte Mathematik und Physik (ZAMP)*, vol. 21, no. 5, pp. 717-742, 1970.

[5] W. Z. Sadeh, H. J. Brauer. Coherent substructure of turbulence nearthe stagnation zone of a bluff body. *Journal of Wind Engineering and Industrial Aerodynamics*, vol. 8(1), no. 59–72, 1981.

[6] P. Bearman. Some measurements of the distortion of turbulence approaching a two-dimensional bluff body. *Journal of Fluid Mechanics*, vol. 53(03), no. 451-467, 1972.

[7] W. Z. Sadeh, P. P. Sullivan. Turbulence amplification in flow about an airfoil. in *ASME 1980 International Gas Turbine Conference and Products Show. American Society of Mechanical Engineers*, 1980.

[8] O. S. Kerr, J. W. Dold. Periodic steady vortices in a stagnation-point flow. *Journal of Fluid Mechanics*, vol. 276, pp. 307-325, 1994.

[9] W.S. Saric, H. L. Reed, E. White. Stability and transition of three-dimensional boundary layers. *Annual Review of Fluid Mechanics*, vol. 35(1), no. 413-440, 2003.

[10] B. B. H. Mueller. Experiments on the laminar-turbulent transition on swept wings. NASA STI Recon Technical Report N, 90:16170, 1988.

[11] K. Hiemenz. Die Grenzschicht an einem in den gleichförmigen Flüssigkeitsstrom eingetauchten geraden Kreiszylinder. PhD Thesis, 1911.

[12] L. Rosenhead. Laminar boundary layers. Clarendon Press, 1963.

[13] E. R. Gowree, C. J. Atkin. Incopressible turbulent flow at the leadingedge of swept wings. *ICAS proceedings*, 2014.

[14] W. Pfenninger. Flow phenomena at the leading edge of a swept wing.*AGARD Recent development in boundary-layer research*, pp. Part IV, 97, 1965.

[15] M. Gaster. On the flow along swept leading edges. *Aeronautical Quarterly*, pp. 18, pp.165, May 1967.

[16] D. Poll. Transition in the infinite swept attachment line boundary layer. *Aero. Q.*, vol. 30, no. 607–629, 1979.

Contact Author Email Address

isabella.fumarola.1@city.ac.uk

Copyright Statement